

# Determination of yttrium iron garnet superexchange parameters as a function of oxygen and cation stoichiometry

W. Noun,<sup>1</sup> E. Popova,<sup>1,\*</sup> F. Bardelli,<sup>2,†</sup> Y. Dumont,<sup>1</sup> R. Bertacco,<sup>3</sup> A. Tagliaferri,<sup>4</sup> M. Tessier,<sup>1</sup> M. Guyot,<sup>1</sup> B. Berini,<sup>1</sup> and N. Keller<sup>1</sup>

<sup>1</sup>*GEMaC, CNRS–UVSQ, 45 Avenue des Etats-Unis, 78035 Versailles, France*

<sup>2</sup>*GILDA-CNR-TASC, c/o ESRF, 6 rue Jules Horowitz, BP 220, 38043 Grenoble, France*

<sup>3</sup>*CNISM and LNESS, Dipartimento di Fisica, Politecnico di Milano, Via Anzani 42, 22100 Como, Italy*

<sup>4</sup>*CNISM and Dipartimento di Fisica, Politecnico di Milano, Piazza Leonardo da Vinci 32, 20133 Milano, Italy*

(Received 28 July 2009; revised manuscript received 6 November 2009; published 9 February 2010)

In this work, we describe the consequences of oxygen and metal-ion deficiency for the magnetic properties of a magnetic oxide in bulk and thin-film form. The influence of the off stoichiometry on valence of the iron atoms and the local structural configuration of these atoms is investigated in correlation with the magnetic Curie temperatures and the associated microscopic parameters, such as the exchange integrals. Combining both structural information obtained by x-ray absorption spectroscopy at Fe *K* edge and exchange integrals as determined from temperature-resolved magneto-optical magnetometry, we show that the electron-transfer integrals, underlying the superexchange interaction, control the global dependence of the Curie temperature on stoichiometry as should be expected. The determination of the electron-transfer integrals allows also the confirmation that metal-ion deficiencies in off-stoichiometric yttrium iron garnet (OS YIG) films lead to a significant increase in the magnetization (as observed experimentally). That can only be explained when considering a preferential site occupation of the iron vacancies on octahedral sites in agreement with our earlier work on OS YIG films [Y. Dumont *et al.*, Phys. Rev. B **76**, 6 (2007)]. Furthermore, the combination of the experimentally determined iron valence with the Fe<sub>*a*</sub>-O-Fe<sub>*d*</sub> bonding angle and the exchange integrals allows for the direct determination of the crystal electric field parameter and the Coulomb repulsion energy as a function of the stoichiometry of the YIG films.

DOI: [10.1103/PhysRevB.81.054411](https://doi.org/10.1103/PhysRevB.81.054411)

PACS number(s): 75.30.Et, 61.05.cj, 78.20.Ls

## I. INTRODUCTION

Nowadays, complex oxides in thin-film form attract a lot of research efforts in order to develop materials with interesting and useful functional properties. Understanding and controlling their defects at a nanoscale level is necessary for integration of these materials into modern technologies based on oxide thin films, heterostructures, or interface properties (also called oxide electronics<sup>1</sup>). It became possible to identify the nature of defects in oxides with the combination of local and macroscopic measurements. Such correlated macroscopic and local structure studies give insights in several functional oxides that have already been extensively investigated for decades. One of these functional oxides, yttrium iron garnet (Y<sub>3</sub>Fe<sub>5</sub>O<sub>12</sub> or YIG), is a widely studied ferrite due to its impact in microwave and magneto-optical device technology. The magnetic and structural properties of pure and substituted YIG have been intensively studied<sup>2</sup> in order to improve its magnetic properties at high frequencies. It was demonstrated that, generally, defects in bulk YIG deteriorate Curie temperature and macroscopic magnetization, except in the case of yttrium substitution by a magnetic rare-earth element. However, it has been reported recently that in the case of polycrystalline relaxed thin films of pure YIG, it is possible to increase significantly the saturation magnetization and Curie temperature inducing oxygen and cation defects.<sup>3–7</sup> These effects were surprising in the garnet structure that is well known for its structural stiffness. Several hypotheses explaining mechanisms of magnetic properties variation with the stoichiometry were considered: for ex-

ample, changes in iron valence and/or in site occupancy.<sup>5</sup> However, using macroscopic measurements only, it is difficult to discriminate between several effects that may lead to such variations in an oxide. The microscopic reason for increasing Curie temperature and magnetization in off-stoichiometric YIG still needs to be understood.

The crystallographic lattice of yttrium iron garnet is cubic centered (*Ia3d*) and contains eight Y<sub>3</sub>Fe<sub>5</sub>O<sub>12</sub> formula units in each elementary lattice cell. The general formula of YIG is {Y<sub>3</sub>}[Fe<sub>2</sub>](Fe<sub>3</sub>)O<sub>12</sub> where the symbols {}, [], and () indicate, respectively, the dodecahedral, octahedral (*a*), and tetrahedral (*d*) sites in the oxygen compact cubic structure. The structure of stoichiometric YIG does not present interstitial sites. The ferrimagnetism of YIG is explained by the existence of two nonequivalent magnetic sublattices composed of iron atoms in 16 octahedral and 24 tetrahedral sites coupled antiferromagnetically. The effective magnetic moment is 5μ<sub>B</sub> per iron atom and the resulting magnetization is around 1750 G at room temperature.

The Curie temperature (*T<sub>C</sub>*) of YIG thin films is found to be dependent on oxygen stoichiometry<sup>4,5</sup> and, indirectly, on cation stoichiometry.<sup>5</sup> It increases when the oxygen content is different from stoichiometric and with increasing metal-ion deficiency. A similar dependence of *T<sub>C</sub>* with stoichiometry has been recently reported for bismuth iron garnet.<sup>7</sup> The Curie temperature of bulk garnet samples has been studied for different cationic substitutions in dodecahedral, octahedral, and tetrahedral sites<sup>8</sup> keeping (Y<sub>3–*x*</sub>R<sub>*x*</sub>)/(Fe<sub>5–*x*</sub>M<sub>*x*</sub>)=0.6, where *R* and *M* are the substituting ions in dodecahedral and octahedral/tetrahedral sites, respectively. However, no inves-

tigations have been performed for  $Y/Fe \neq 0.6$ .

Stoichiometric YIG is a good insulator, well described in an ionic model where cations (Y and Fe) are trivalent and oxygen is divalent. Formally, the change in Y/Fe ratio or in oxygen content leads to iron valences different from three, i.e., the creation of  $Fe^{2+}$  or  $Fe^{4+}$  ions, which act, respectively, such as donors or acceptors. The presence of these ions can affect the magnetic properties of YIG as well.  $Fe_d-O-Fe_a$  distances and angles are modified by the valence change as well as by the lattice distortion created by cation or anion vacancy. However, this has not been experimentally proven and x-ray absorption spectroscopy (XAS) measurements offer unique opportunities to this scope. XAS is a technique giving information on the local structure and on the electronic states in condensed matter. X-ray absorption spectra are obtained by tuning the photon energy in a range where bound electrons can be excited. Two regions of x-ray absorption spectra can be identified: x-ray absorption near-edge structure (XANES) and extended x-ray absorption fine structure (EXAFS).

The XANES region is located at low values of kinetic energy ( $E_{absorption} - E_{edge} \leq 50$  eV). In this case the photoelectron is characterized by a long lifetime, with a mean-free path of several tens of angstroms. Therefore, the photoelectron can be diffused in multiple ways by the surrounding atoms and the atoms located at several angstroms from the absorbent atom. Consequently, the XANES measurements of a specific element absorption edge contain information allowing characterization of the oxidation state of the absorbing element, the geometry of the site in which it is located and also its local environment (nearest neighbors).

For high values of the kinetic energy ( $E_{absorption} - E_{edge} > 50$  eV approximately), the photoelectron lifetime is short and the processes of simple scattering (or backscattering) are dominant. In consequence, EXAFS measurements give the information about the nature of the nearest neighbors as well as about the interatomic distances and angles.

Despite the enormous amount of publications concerning the structural, magnetic, electrical, and optical properties of bulk materials and thin films of the pure and substituted YIG,<sup>2,8-11</sup> no detailed EXAFS studies and analysis have been performed.

In this paper, we will concentrate on the consequences of oxygen and metal-ion deficiency for the valence of the iron atoms, for their local structural configuration in correlation with the magnetic Curie temperatures and the associated microscopic parameters, such as the exchange integrals. The study has been carried out on both bulk samples with different Y/Fe ratios and thin films grown at different oxygen pressures. In fact, under certain thin-film preparation conditions, oxygen-content variation is accompanied by the slight cation off stoichiometry,<sup>5</sup> to some extent analogous to that of bulk samples. Combining both structural information obtained by EXAFS and exchange integrals as determined from magneto-optical magnetometry at variable temperature, we show that the electron-transfer integrals, underlying the superexchange interaction, control the global dependence of the Curie temperature on stoichiometry as should be expected. The determination of the electron-transfer integrals allows also confirming that metal-ion deficiencies in these

off-stoichiometric films lead to a significant increase in the magnetization. This can only be explained when considering a preferential site occupation of the iron vacancies on octahedral sites in agreement with our earlier work on off-stoichiometry yttrium iron garnet films.<sup>3-6,12</sup> Furthermore, the combination of the experimentally determined iron valence with the bonding angle and the exchange integrals allows the determination of the crystal electric field parameter  $D_q$  as a function of the stoichiometry of the YIG films.

## II. EXPERIMENT

### A. Bulk sample preparation and characterization

Bulk YIG samples with different cation ratio Y/Fe were prepared by traditional ceramic process. High purity (5N)  $Y_2O_3$  and  $Fe_2O_3$  are mixed in the desired proportion and then milled for a long time by a specially developed nonpolluting setup.<sup>13</sup> The obtained powder then pressed into pellets and sintered at 1200 °C for several days in air flow. The cation ratio Y/Fe is checked using chemical titration methods. The sample having Y/Fe=0.574 is prepared without milling. For the EXAFS measurements the single phase and dense pellets are grinded and pressed into smaller pellets compatible with the x-ray absorption measurement setup.

X-ray diffraction measurements were performed in order to determine an average sample lattice parameter  $a$ . As the lattice-parameter variation for different Y/Fe is extremely small, much care has been taken to make the measurements as precise as possible. The grinded sample powder was mixed with a reference powder. All the peaks in  $\Theta$ - $2\Theta$  scans were deconvoluted to extract  $\Theta$  values corresponding to  $K_{\alpha 1}$  radiation. Then the  $\Theta$  values were normalized to the reference peak position. The lattice parameter  $a$  was calculated from each diffraction peak, then the average  $a$  value was determined for a sample. Independently, Rietveld refinement of the lattice parameter was performed. The lattice parameters obtained from Rietveld analysis corresponded to those determined from peak deconvolution. No more useful information, such as yttrium or iron concentration, could be extracted from the refinement because of the used measurement configuration. Also, oxygen concentration in the samples cannot be determined from x-ray measurements. Figure 1(a) presents the average lattice parameter as a function of Y/Fe ratio. The following observations could be made: (i) for the Y/Fe ratio close to the stoichiometric value of 0.6, the lattice parameter is very close to the bulk stoichiometric (BS) value (12.376 Å) reported in the literature; (ii) the relative lattice variation is very small in the investigated range of Y/Fe ratios; (iii) there is no clear dependence of  $a$  on Y/Fe ratio, therefore, no direct influence of this ratio on lattice size can be evidenced. For these reasons, in the following we present the results for bulk samples as a function of Y/Fe ratio rather than lattice parameter.

The Curie temperature was measured using a vibrating sample magnetometer equipped with a custom-designed high-temperature furnace. The temperature sensor was fixed on a sample surface to obtain the precise value of the temperature. The sensor calibration was cross checked performing permeability measurement on one of the samples. Mag-

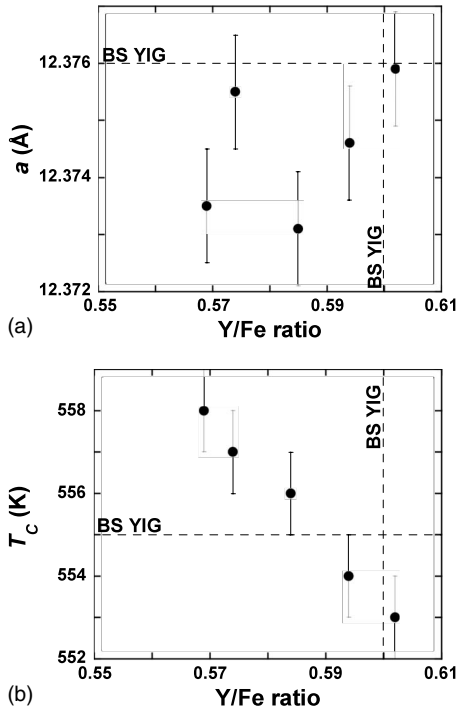


FIG. 1. Variation in the (a) average lattice parameter and (b) Curie temperature of bulk YIG as a function of cation stoichiometry. The corresponding values for bulk stoichiometric (BS) YIG are given for comparison.

netic moment of each sample was measured in saturation field with temperature steps of 1 K in the vicinity of  $T_C$ . The results are shown in Fig. 1(b) as a function of Y/Fe ratio. The value of  $T_C$  from the literature (555 K) is given for the reference. The slight difference between the Curie temperature for an almost stoichiometric sample with  $Y/Fe \approx 0.6$  and the reference value may be due to the difference in thermometry setup. It is clear from Fig. 1(b) that the Curie temperature changes very slightly in the studied Y/Fe region; in particular, it decreases with Y/Fe stoichiometry approaching its theoretical value of 0.6.

**B. Thin-film preparation and characterization**

The polycrystalline YIG thin films have been prepared by pulsed laser deposition from a polycrystalline target of stoichiometric YIG as described in Refs. 3–5 and 12. The films were grown on amorphous quartz substrates using a Nd:YAG laser with the wavelength of 355 nm. The laser beam was focused onto the target with a fluency of 8 J/cm<sup>2</sup> maintained constant during the deposition time of 4 h. The distance between the target and the substrate was fixed to 50 mm. For the purpose of this study, all YIG samples were prepared at a constant substrate temperature of 850 °C and in oxygen pressure that was varied between 15 and 200 mTorr.

The lattice parameter determined from x-ray diffraction measurements is presented in Fig. 2(a) as a function of oxygen pressure. This dependence  $a(P_{O_2})$  is linear and is comparable to the one observed by Dumont *et al.*<sup>5</sup> Therefore, the lattice parameter in thin films seems to be directly related to

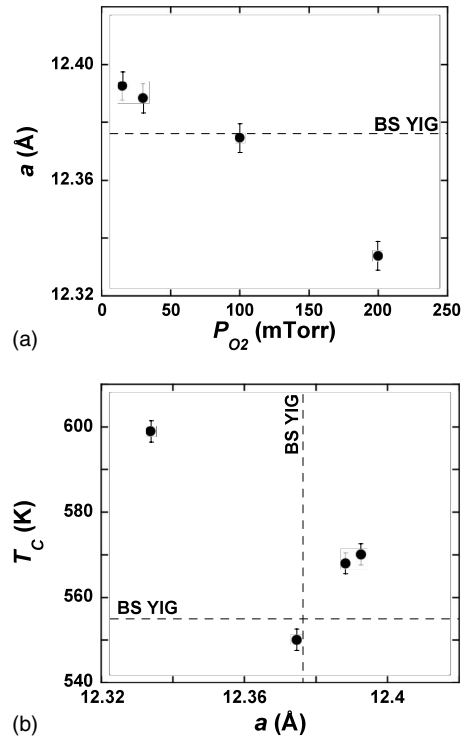


FIG. 2. Variation in the (a) average lattice parameter as a function of the oxygen pressure during the deposition and in (b) Curie temperature as a function of the lattice parameter. The corresponding values for BS YIG are given for comparison.

oxygen stoichiometry. The effects of eventual strain induced by the substrate on the film structure can be excluded as all the films were deposited on amorphous quartz substrates and found to be polycrystalline and completely relaxed. No crystallographic texture has been evidenced. All the following results obtained for thin films will be presented as a function of  $a$ . The stoichiometric lattice parameter is measured for the sample prepared at 100 mTorr. The difference in the pressure value giving a stoichiometric sample between the present results and our previous results<sup>5</sup> is due to the changes in oxygen injection setup. The relative variation in  $a$  in thin nonstoichiometric films is about 25 times greater than in bulk nonstoichiometric samples for the studied ranges of, respectively, oxygen and cation off stoichiometry.

Curie temperatures for the thin films were determined from temperature-dependent Faraday rotation measurements that have been performed using a custom-designed magneto-optical magnetometer.<sup>14</sup> Magneto-optical hysteresis was measured at several temperature values with a step of 10 K in the vicinity of  $T_C$ . Analysis of the magneto-optical hysteresis loops allows determining the thermal variation in the magnetization and the Faraday rotation (see Refs. 5 and 7 for more details). The results for the Curie temperatures are presented in Fig. 2(b). The Curie temperature of a stoichiometric sample is very close to that of bulk stoichiometric  $T_C$  value. As the lattice parameter increases above or decreases below the corresponding value of bulk stoichiometric YIG, the Curie temperature of the film increases significantly and reaches the maximum of  $\Delta T_C/T_C \approx +9\%$ . The results are comparable to those already published by our group.<sup>5</sup> The

relative  $T_C$  variation for the off-stoichiometric YIG films is ten times larger than the corresponding  $T_C$  variation observed for the cation off-stoichiometric bulk samples.

### C. XAS setup

XAS technique allows studying the local atomic environment (up to 6–8 Å) around a given absorber ion (Fe, in the present case). The near-edge part of the absorption spectra (XANES) provides information on the absorber oxidation state and site geometry whereas local structural information on the absorber surroundings (neighboring atomic species, bond distances, coordination, and disorder) are extracted from the extended part (EXAFS).

XAS measurements were performed at the Fe  $K$  edge (7112 eV) at the beamline GILDA (BM-08) at the European Synchrotron Radiation Facility (ESRF) in Grenoble (France).

The main characteristic of the beamline optics is a fixed exit monochromator mounting a couple of Si(311) crystals and Pd mirrors for efficient harmonic rejection. The monochromator is equipped with a dynamic sagittal focusing system increasing the beam intensity on the sample. The beam-spot size on the sample was about  $500H \times 250V \mu\text{m}^2$ , the energy resolution about 0.5 eV, and the photon flux was about  $5 \times 10^{10}$  ph/s at 7.2 keV. In order to reduce the thermal contribution to the Debye-Waller factors, all samples were measured at liquid nitrogen temperature (77 K). Bulk YIG reference spectra were acquired in transmission geometry, i.e., measuring the intensity of the beam incident on the sample ( $I_0$ ) and the transmitted one ( $I_t$ ), using ionization chambers. The absorption spectra are then calculated as  $\mu(E) = \ln(I_0/I_t)$ . Fluorescence yield of YIG thin-film samples was measured using a 13-element HP-Ge detector (ORTEC). A minimum of two spectra were collected for each sample and averaged to obtain high-quality data. For each spectrum a simultaneous Fe-foil reference spectra was measured in order to have accurate energy calibration.

Standard procedures were followed to extract the EXAFS signal and refine the data.<sup>15</sup> Data refinements were performed on the back-transformed EXAFS spectra ( $q$  space), applying the standard XAFS formula. The atomic cluster was created using the ATOMS code exploiting structural information reported in MYNCRYST database<sup>16</sup> for YIG crystallographic structure.<sup>17</sup> These data were used to create atomic cluster for amplitude and phase backscattering function calculations (using FEFF8 code), and as starting points for the refinements. The minimization code is based on the MINUIT routines developed at the CERN. During the minimizations, the many-body loss factor and a global experimental energy shift ( $\Delta E$ ) have been kept fixed to values optimized from comparison with Fe-foil and Fe-oxides references, and a first-shell-limited analysis, respectively. The coordination numbers have also been kept fixed to theoretical values, in order to reduce the correlation between the parameters. Only bond distances, Debye-Waller factors, and a global experimental energy shift  $\Delta E$  were let free to vary. Errors on parameters were calculated using the MINOS subroutine from the MINUIT package, which take into account the correlation between parameters.

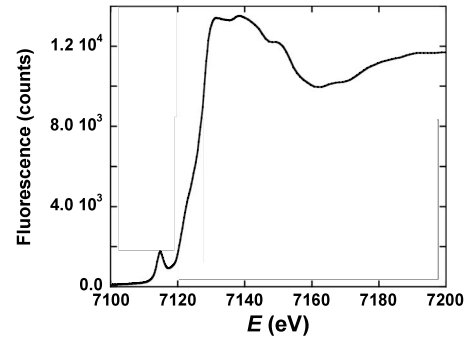


FIG. 3. Absorption spectrum of a YIG thin film prepared at 15 mTorr of oxygen pressure. The curve was normalized for the incoming x-ray intensity. The pre-edge background has been adjusted.

### III. IRON-ION VALENCE FROM XANES MEASUREMENTS

In our previous work<sup>5</sup> we have observed a significant increase (up to 120%) of the saturation magnetization  $M_s$  for a narrow window in oxygen off stoichiometry. We have issued two hypotheses to explain this magnetization “overshoot:” (i) iron valence change and/or (ii) site-occupancy variation. However, with the data we disposed it was impossible to discriminate between two proposed explanations. The XANES measurements of iron valence in the nonstoichiometric samples should allow determining which hypothesis was closer to the reality.

The experimental absorption spectra at iron  $K$  edge are presented in Fig. 3. They are similar to those observed for compounds containing  $\text{Fe}^{3+}$  (see, for example, Ref. 18) and consist of three features: a pre-edge peak at around 7112 eV, a broad shoulder around 7122 eV, and an edge crest at 7130 eV. The pre-edge is principally due to the  $1s \rightarrow 3d$  electric quadrupole transitions in the tetrahedral site. This transition is normally forbidden in case of a centrosymmetric octahedral site. In practice, there is a small contribution from the iron ions in octahedral sites to the pre-edge as shown for YIG samples.<sup>19</sup> This contribution is quite difficult to quantify, as there is a high uncertainty (about 10%) in the procedure of the deconvolution of a low intensity pre-edge from the experimental XANES spectrum.

The value of the pre-edge energy corresponds to a transition of an electron from a core state  $1s$  to the first empty energy level  $3d$  ( $\text{Fe } 1s^2 \dots 3d^5 \rightarrow \text{Fe } 1s^1 \dots 3d^6$ ). There is a difference in energy at which this transition occurs depending on iron-valence state and/or on the site that iron-ion occupies.<sup>18–20</sup> Several transitions are possible between  $1s$  and  $3d$  levels due to the hybridization and consequent multiplicity of possible final states. As the number of transitions depends on the oxidation state and on the coordination number of iron ions,<sup>21</sup> there should be several corresponding contributions into the pre-edge region. Therefore, the shape of the pre-edge and the area below the pre-edge part of the absorption curve should differ according to the iron-valence state and the site occupancy. Great attention should also be paid to the crystallographic distortion as it can modify the energy of the levels and cause supplementary electron transitions.

In the case of iron-ion mixture on each site ( $\text{Fe}^{2+}/\text{Fe}^{3+}$  or  $\text{Fe}^{3+}/\text{Fe}^{4+}$ , as we expect from our previous investigations<sup>5</sup>),

the energy of  $1s \rightarrow 3d$  transition varies.<sup>18</sup> The pre-edge energy in this case is situated between the energy values corresponding to  $\text{Fe}^{2+}$  and  $\text{Fe}^{3+}$  or  $\text{Fe}^{3+}$  and  $\text{Fe}^{4+}$ , respectively. The energy shift from pure  $\text{Fe}^{2+}$  increases linearly with the increasing concentration of another type of iron ions ( $\text{Fe}^{3+}$  or  $\text{Fe}^{4+}$ ) in a sample.<sup>19,22</sup> In the case of iron-valence mixture, the energy, the shape, and the intensity of the pre-edge changes.<sup>19</sup>

In most of the experimental works the energies corresponding to  $\text{Fe}^{2+}$  and  $\text{Fe}^{3+}$  are around, respectively, 7112 and 7114 eV (see, for example, Ref. 19). Therefore, the difference between the energy of these two valence states is 2 eV (Ref. 22) but can be also as low as 1.6 eV. It is important to mention that in the above cited papers all  $\text{Fe}^{2+}$  or  $\text{Fe}^{3+}$  ions are situated in one type of site: either octahedral or tetrahedral. The study performed by Waychunas *et al.*<sup>18</sup> points out that the difference in the pre-edge energies of  $\text{Fe}^{2+}$  or  $\text{Fe}^{3+}$  ions is not the same when they are located in tetrahedral or octahedral sites. For an octahedral site this difference is 3 eV while for a tetrahedral site it is between 1 and 2 eV. In the case of YIG both types of site are present and  $\text{Fe}^{2+}$  or  $\text{Fe}^{3+}$  ions can occupy both sites.<sup>2</sup> Therefore, this kind of analysis becomes difficult.

In literature, the pre-edge has been adjusted with a variety of different line shapes: Gaussian, pseudo-Voigt, polynomial, etc.<sup>19–21</sup> Supposing the presence of both types of site (octahedral and tetrahedral) and their occupation by either  $\text{Fe}^{2+}$  or  $\text{Fe}^{3+}$ , the choice of a particular line-shape function only allows for a reproducible determination of pre-edge energies and their relative weight. In the following the average value of the pre-edge energy obtained by fitting the pre-edge with a pseudo-Voigt function will be used.

The average valence of iron in a sample can thus be determined measuring the pre-edge shift from the energy corresponding to the  $\text{Fe}^{2+}$  or  $\text{Fe}^{3+}$  reference pre-edge. Figures 4(a) and 4(b) present the pre-edge shifts of the samples and the reference of  $\text{Fe}^{3+}$  ions (hematite  $\text{Fe}_2\text{O}_3$ ) with respect to the energy position of the pre-edge of  $\text{Fe}^{2+}$  reference (hercynite  $\text{FeAl}_2\text{O}_4$ ), which is measured to be at 7112.61 eV. The dashed lines show the relative energy of the pre-edge of two references. The shaded zone around the dashed lines takes into account the error bars of the reference measurements. It is evident that the average valence in bulk samples is smaller than  $\text{Fe}^{3+}$  whatever the value of the Y/Fe ratio. This implies the presence on a certain amount of  $\text{Fe}^{2+}$  ions. When the valence of iron increases, the pre-edge shifts to higher energies:  $E(\text{Fe}^{2+}) < E(\text{Fe}^{3+}) < E(\text{Fe}^{4+})$ . We assume that the presence of  $\text{Fe}^{2+}$  excludes the presence of  $\text{Fe}^{4+}$ . In the case of a mixed valence, ( $\text{Fe}^{2+} + \text{Fe}^{3+}$ ) or ( $\text{Fe}^{3+} + \text{Fe}^{4+}$ ), the pre-edge is situated between the energies corresponding to  $\text{Fe}^{2+}$  and  $\text{Fe}^{3+}$  or  $\text{Fe}^{3+}$  and  $\text{Fe}^{4+}$ , respectively. If we consider a linear shift in the pre-edge energy with increasing fraction of  $\text{Fe}^{2+}$  ions, then the quantity of  $\text{Fe}^{2+}$  decreases with increasing Y/Fe ratio and its fraction can be estimated from Fig. 3(a) to be between 30% for Y/Fe=0.569 and 26% for Y/Fe=0.602. The detection of  $\text{Fe}^{2+}$  ions in a cation-stoichiometric sample indicates the presence of oxygen vacancies in bulk samples. However, the experimental values of the lattice parameters in bulk samples hardly suggest any deviation from oxygen stoichiometry as they are very close to the stoichiometric bulk

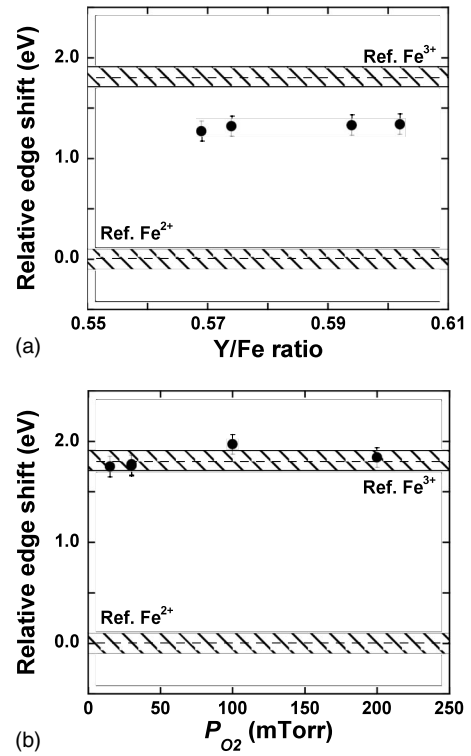


FIG. 4. Shift of absorption pre-edge with respect to  $\text{Fe}^{2+}$  and  $\text{Fe}^{3+}$  references for (a) bulk YIG and (b) YIG thin films.

value [see Fig. 1(a)]. At present, there is no plausible explanation of this contradiction. We could only mention several effects that may contribute in a complex way to the lattice-parameter value: (i) change in ionic radii related to the valence change from  $\text{Fe}^{3+}$  to  $\text{Fe}^{2+}$  (Ref. 23) and/or (ii) change in local structure either due to missing oxygen atoms or due to angle  $\text{Fe}_d\text{-O-Fe}_a$  modification. It should also be noted that different processes of sample synthesis in bulk or thin-film form may lead to the fundamental differences in the way the oxygen and cation vacancies are created.

For the thin films we expect to observe the pre-edge variation with oxygen pressure. According to its properties, the sample prepared at 100 mTorr is considered to be oxygen stoichiometric. Therefore, all iron ions should have the valence 3+. The samples prepared at  $P_{\text{O}_2} < 100$  mTorr have oxygen vacancies that must lead to the formation of  $\text{Fe}^{2+}$  ions. On the contrary, the sample grown at  $P_{\text{O}_2} > 100$  mTorr has the cation deficiency presumably resulting in the appearance of  $\text{Fe}^{4+}$  ions.<sup>5</sup> However, whatever value of the oxygen pressure is, experimentally we observe that the valence of all films is very close to 3+ [Fig. 4(b)].

The saturation magnetization measurements on cation nonstoichiometric samples (not shown here) exhibit no overshoot for any samples in the studied Y/Fe ratio region:  $M_S < M_S^{\text{stoich}}$  for Y/Fe < 0.585 and  $M_S \approx M_S^{\text{stoich}}$  for Y/Fe > 0.585. Meanwhile, as shown above, roughly 30% of iron ions in *all bulk samples* of the series have valence of 2+. In addition, the overshoot of saturation magnetization is observed in oxygen nonstoichiometric thin-film specimens<sup>5</sup> while all the iron ions are 3+ as measured by XANES. These experimental results allow concluding that  $M_S$  variation is

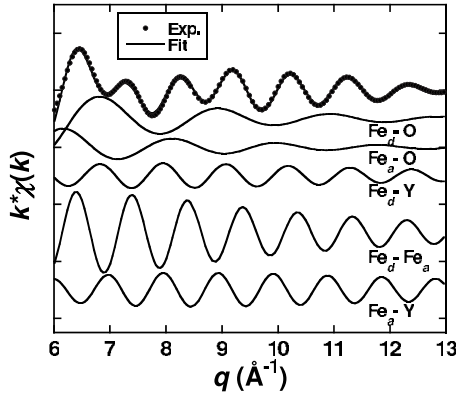


FIG. 5. Back-transformed (1–4.5 Å) experimental EXAFS spectrum (dots) for a YIG thin film (prepared at 15 mTorr of oxygen pressure) compared to fit (line). Also reported (lines, shifted) are the contribution of the coordination shells included in the minimization procedure:  $Fe_{d,a}$ -O,  $Fe_{d,a}$ -Y, and  $Fe_d$ - $Fe_a$ .

governed by iron site-occupancy change rather than iron-valence variation.

IV. EXAFS MEASUREMENTS

EXAFS data, containing the information about local structure around an absorbing atom, were extracted from experimental absorption spectra. The refinements of the obtained XAS oscillations were performed using five possible single-scattering paths of a photoelectron from an absorbing to a scattering atom. The five used paths ( $Fe_{a,d}$ -O,  $Fe_{a,d}$ -Y, and  $Fe_a$ - $Fe_d$ ) are shown in Fig. 5 in the  $q$ -wave vector space. They are represented with continuous lines and are shifted for clarity.  $Fe_{a,d}$  stands for the iron atom in, respectively, octahedral or tetrahedral oxygen coordination. The experimental data are given in Fig. 5 using a dotted line and the final adjustment is represented with a superposed continuous line. It is clear that the fit is quite close to the experimental data.

Refinements allow extracting five distances between iron atoms and nearest or next-nearest neighbors. These distances are plotted in Fig. 6 for bulk samples and in Fig. 7 for thin-film samples. All the distances are greater than those expected from interatomic distance calculations for stoichiometric YIG.<sup>16,17</sup> In the following focus will be made on the relative variations between the samples with different Y/Fe ratio or oxygen content.

In the bulk samples the distances Fe-O seem not to vary too much with Y/Fe ratio. On the contrary, Fe-Fe and Fe-Y distances increase with Y/Fe approaching stoichiometric ratio. The relative Fe-Fe distance variation in bulk samples is  $4 \times 10^{-3}$ . For the thin films all three distances obtained from EXAFS measurements increase with increasing lattice parameter measured by x-ray diffraction until  $a = a_{stoich}$ , then decrease for  $a > a_{stoich}$ . The relative Fe-Fe distance variation is  $3 \times 10^{-3}$ , which is the same order of magnitude as in bulk YIG in the studied nonstoichiometry region. The apparent contradiction between the increase in the average lattice parameter  $a$  and the decrease in local interatomic distances can

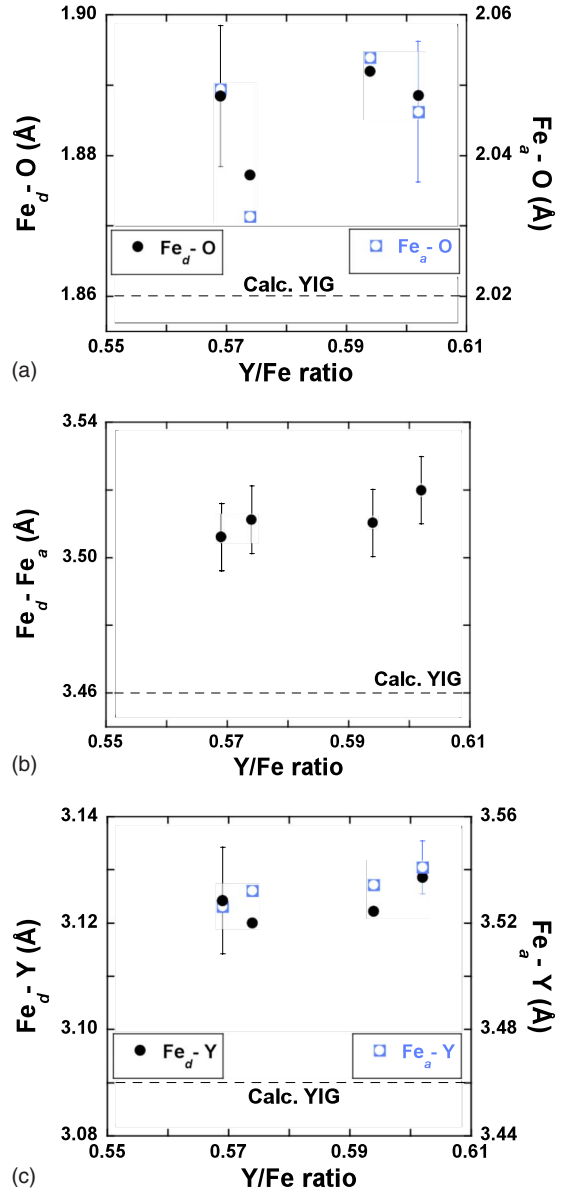


FIG. 6. (Color online) Local distances in bulk YIG lattice with variable cation stoichiometry.  $Fe_{d,a}$  stands for the iron atom in, respectively, tetrahedral or octahedral oxygen coordination. Dashed line represents the corresponding interatomic distance calculated from Refs. 16 and 17.

probably be explained by the creation of oxygen vacancies breaking Fe-Fe superexchange bonds. This leads to the decrease in the average local Fe-Fe and Fe-O distances deduced from EXAFS measurements. It should be pointed out that x-ray diffraction measurements give the “macroscopic”  $a$  parameter averaging the lattice distortions while EXAFS allows determining local distances and distortions.

V. CORRELATION BETWEEN THE LOCAL DISTORTION MEASURED BY EXAFS AND THE CHANGE IN THE CURIE TEMPERATURE

It is possible to calculate the angle  $\alpha$  between iron magnetic moments using the measured distances Fe-O and Fe-Fe.

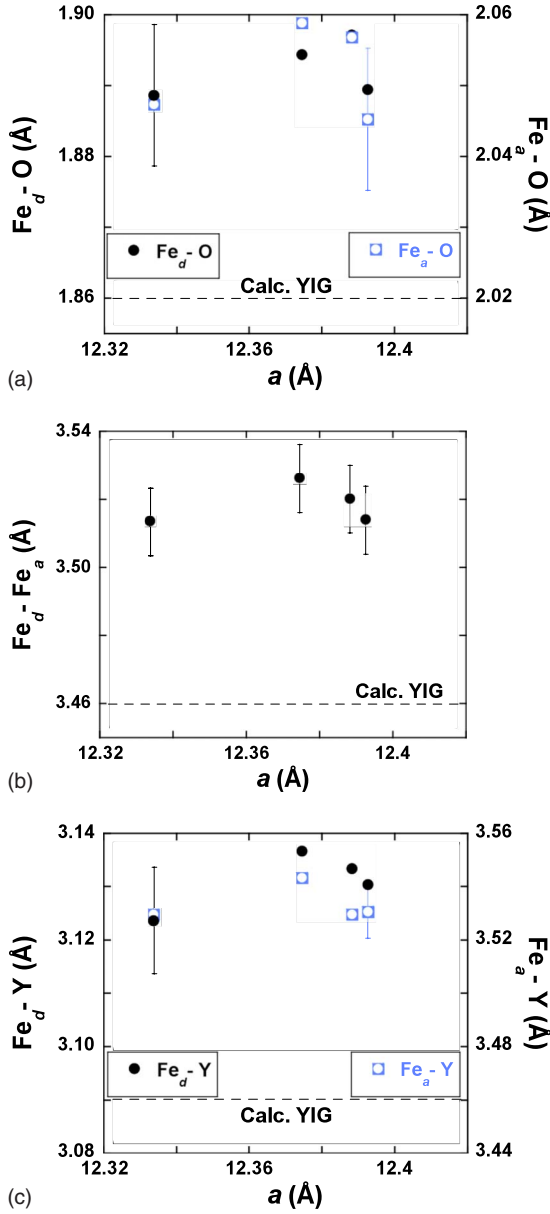


FIG. 7. (Color online) Local distances in thin-film YIG lattice with variable oxygen stoichiometry.  $Fe_{d,a}$  stands for the iron atom in, respectively, tetrahedral or octahedral oxygen coordination. Dashed line represents the corresponding calculated interatomic distance (Refs. 16 and 17).

Figure 8 shows  $\alpha(Fe_d-O-Fe_a)$  as a function of cation and oxygen stoichiometry. A schematic representation of the angle is shown in Fig. 9(a). It should be noted that the sample with  $Y/Fe=0.574$  is prepared in the conditions slightly different from three other samples. Therefore, there is a difference in Fe-O distances that results in difference in  $\alpha$  value [Fig. 8(a)]. The relative angle variation for bulk samples is around  $1.7 \times 10^{-2}$ . For the thin films [Fig. 8(b)], the relative angle variation is three times smaller. The stoichiometric  $\alpha$  value is observed for the lattice corresponding to stoichiometry in oxygen.

Taking into account the measured distances Fe-Fe and Fe-O, as well as the calculated angle  $Fe_d-O-Fe_a$ , we can

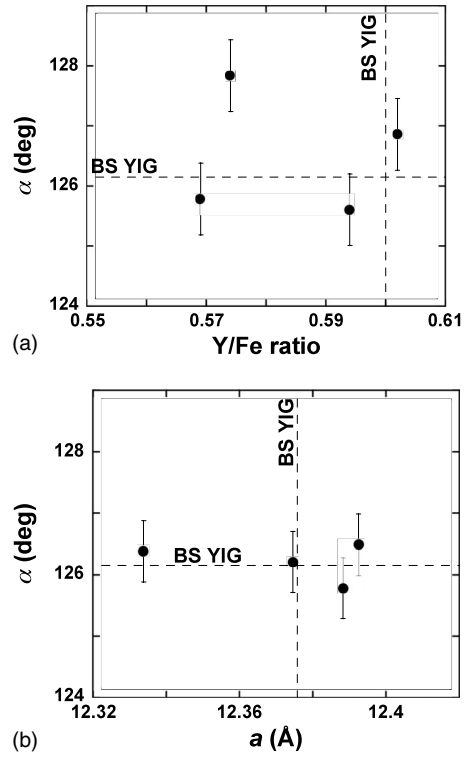


FIG. 8. Angle  $Fe_d-O-Fe_a$  (a) for bulk YIG with variable cation stoichiometry and (b) for thin YIG films with variable oxygen stoichiometry. The corresponding  $\alpha$ ,  $Y/Fe$ , and  $a$  values for BS YIG are given for comparison.

schematically represent the changes induced by nonstoichiometry in cations [Fig. 9(b)] and in oxygen [Fig. 9(c)]. Here the dotted line and pale circles represent the stoichiometric sample with  $T_C^{stoich}$ . In case of nonstoichiometry, when  $\alpha$  stays constant and Fe-Fe distance increases, the exchange integral and, therefore, Curie temperature must decrease. For  $\alpha=const$  and decreasing Fe-Fe,  $T_C$  should increase. For Fe-Fe=const and increasing  $\alpha$ , Curie temperature decreases

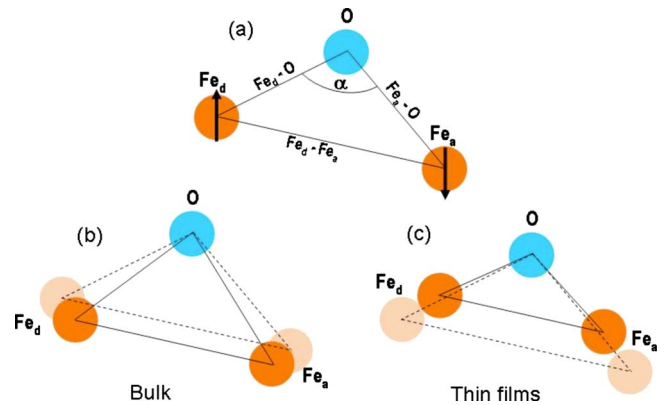


FIG. 9. (Color online) Schematic representation of superexchange coupling between two iron magnetic moments in (a) stoichiometric YIG. Variation in the  $Fe_{d,a}-O$  distances and  $Fe_d-O-Fe_a$  angles in the case of nonstoichiometry in (b) cations and (c) oxygen. The dashed lines and pale circles represent stoichiometric YIG from (a).

while it should increase for decreasing  $\alpha$ . Experimentally, for the bulk samples nonstoichiometric in cations, the angle between iron magnetic moments is smaller than stoichiometric  $\alpha$ . The distance Fe-Fe is also smaller for  $Y/Fe < 0.6$  than for  $Y/Fe = 0.6$ . As mentioned before, the Fe-O distances are considered unchanged. Consequently, the strength of interaction between iron magnetic moments—exchange integral—is greater. Therefore Curie temperature is increased for nonstoichiometric samples. In the thin nonstoichiometric films  $\alpha$  is only slightly larger than  $\alpha_{stoich}$  while Fe-Fe and Fe-O are smaller than in stoichiometric samples. On the overall, the iron atoms are situated closer than in stoichiometric material and Curie temperature increases when the oxygen content deviates from stoichiometric. These results are in perfect agreement with our measurements of Curie temperatures of bulk and thin-film samples. In thin films, the change in Fe-Fe distance is greater than in bulk samples, which corresponds to stronger variation in Curie temperature. The changes in local atom configuration are different for cation and oxygen nonstoichiometry. This former effect is more clearly evidenced in thin films.

The thermal variation in the magnetization, the Faraday rotation  $\theta_F$ , and the Faraday ellipticity  $\varepsilon_F$  can be described in the frame of Néel model as the result of two antiferromagnetically coupled sublattices.<sup>24</sup> The magnetization of  $Y_3Fe_5O_{12}$  can be expressed on a normalized scale as

$$n_B(T) = 3gS_d f_d B_{sd}(x_d^*) - 2gS_a f_a B_{sa}(x_a^*), \quad (1a)$$

where  $B_{si}(x_i)$  represents the Brillouin function of the  $i$ th sublattice ( $i=a, d$ ),

$$B_{si} = \frac{2S_i + 1}{2S_i} \coth\left(\left[\frac{2S_i + 1}{2S_i}\right]x_i\right) - \frac{1}{2S_i} \coth\left(\left[\frac{1}{2S_i}\right]x_i\right) \quad (1b)$$

and with  $n_B = M_S / \mu_B N_A$ ,  $x_d^* = \frac{2S_d}{gT}(j_{dd}n_d + j_{da}n_a)$ ,  $x_a^* = \frac{2S_a}{gT}(j_{aa}n_a + j_{ad}n_d)$  and the exchange integrals  $j_{ij} = J_{ij}/k_B$  in units of kelvin. Here the constants  $f_a$  and  $f_d$  have been introduced to allow for a variation in the zero-temperature magnetization in each sublattice.  $S_i$  represents the spin quantum numbers of the magnetic ions, with  $S_i = 5/2$  for  $Fe^{3+}$  in the high spin state and  $g$  is the spectroscopic splitting factor of each sublattice ( $g=2.0$ ).  $\mu_B$  is the Bohr magneton ( $\mu_B = 9.2741 \times 10^{-24}$  J/T),  $k_B$  is the Boltzmann constant ( $k_B = 1.3807 \times 10^{-23}$  J/K), and  $N_A$  is the Avogadro constant ( $N_A = 6.022 \times 10^{23}$  mol<sup>-1</sup>). The magneto-optical properties can be expressed as

$$\theta_F(T) = C_{V,d} 3gS_d f_d B_{sd}(x_d^*) - C_{V,a} 2gS_a f_a B_{sa}(x_a^*)$$

and

$$\varepsilon_F(T) = C_{E,d} 3gS_d f_d B_{sd}(x_d^*) - C_{E,a} 2gS_a f_a B_{sa}(x_a^*). \quad (2)$$

Equations (1a), (1b), and (2) were integrated into a non-linear least-mean-square fitting algorithm using a self-consistent determination of each sublattice magnetization for the adjustable parameters (e.g.,  $j_{ij}$  with  $i, j = a, d$ ), see Ref. 7 for more details.

The obtained fitting for a sample grown at 200 mTorr of partial oxygen pressure is given in Fig. 10(a), where the

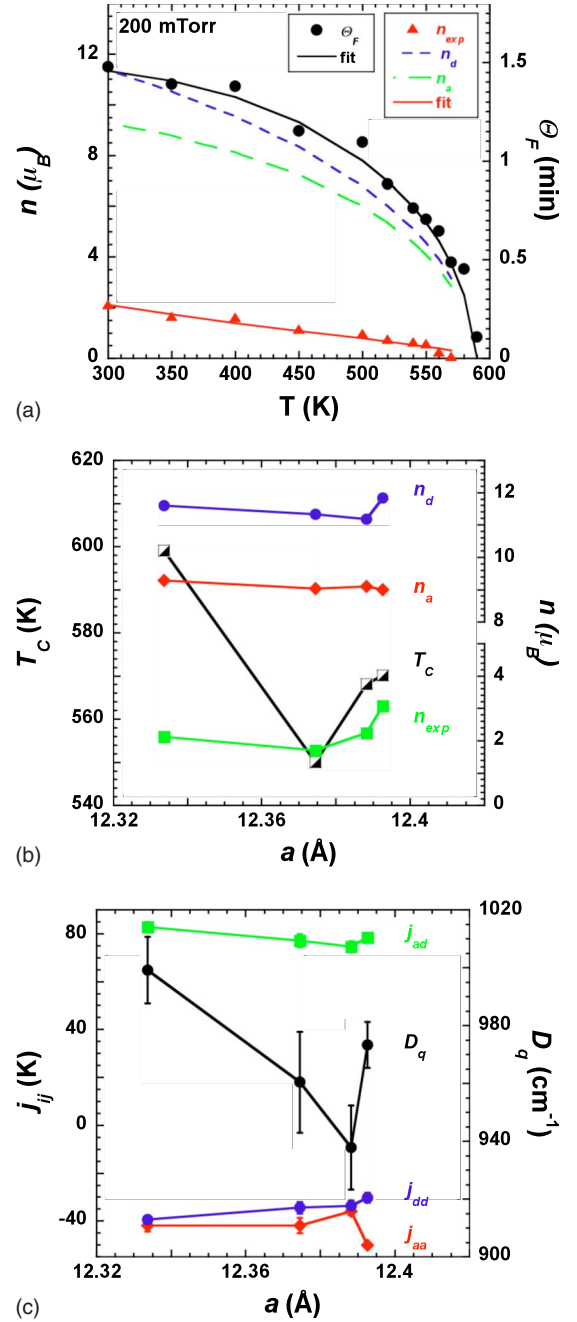


FIG. 10. (Color online) (a) Thermal variation in the Faraday rotation (solid circles), the magnetization (triangles), the resulting fits of the magnetization modeling (see text) and the calculated sublattice magnetizations ( $n_a$  and  $n_d$ —dashed-dotted and dashed lines, respectively). (b) Variation in  $T_C$ , of the experimentally determined magnetization  $n_{exp}$  and the sublattice magnetizations,  $n_a$  and  $n_d$ , with the lattice parameter. (c) Variation in the three exchange integrals,  $j_{aa}$ ,  $j_{dd}$ , and  $j_{ad}$  compared to the calculated variation in the crystal-field parameter  $D_q$  as a function of the lattice parameter.

magnetization, the Faraday rotation, and the Faraday ellipticity have been adjusted. The figure shows the calculated thermal variations for  $M_S$ ,  $\theta_F$ , and  $\varepsilon_F$  and the two-sublattice magnetizations of the tetrahedral and octahedral sublattice (dashed lines). The experimentally determined Curie temperatures as a function of the lattice parameter are displayed

in Fig. 10(b) together with the adjusted overall magnetization,  $n_{exp}$ , and the two-sublattice magnetizations,  $n_a$  and  $n_d$ . For off-stoichiometric samples the Curie temperatures and the global magnetization  $n_{exp}$  are enhanced over the values for a sample with stoichiometric lattice parameter. Figure 10(c) gives the results of this analysis for the exchange integrals  $j_{aa}$ ,  $j_{dd}$ , and  $j_{ad}$  as a function of the oxygen pressure applied during the growth of the films.

Both  $j_{aa}$  and  $j_{dd}$  have negative values characteristic of ferromagnetic interactions whereas  $j_{ad}$  is positive, revealing the expected antiferromagnetic intersublattice coupling. For our YIG films, typical values of  $-42 \pm 7$  K ( $-3.5 \pm 0.6$  meV),  $-30 \pm 5$  K ( $-2.5 \pm 0.4$  meV), and  $78 \pm 5$  K ( $6.5 \pm 0.4$  meV) are obtained for  $j_{aa}$ ,  $j_{dd}$ , and  $j_{ad}$ , respectively. The corresponding energies for YIG are  $-65$  K ( $-5.6$  meV),  $-30$  K ( $-2.5$  meV), and  $97$  K ( $8.4$  meV).<sup>25</sup> Globally, the relative values for the off-stoichiometric YIG films are close to those of bulk YIG. However, one realizes that, in particular, the  $j_{dd}$  exchange integral is hardly affected by the off-stoichiometry whereas both the  $j_{aa}$  and the  $j_{ad}$  are smaller than the bulk values. In average the exchange integrals are weakened by the deficiencies both in oxygen and in cations of the off-stoichiometric films. However, even if the dominant antiferromagnetic exchange integral  $j_{ad}$  is significantly weakened compared to the bulk values, the Curie temperature is increased [see Fig. 2(b)]. The Curie temperature of a two-sublattice system is expressed by<sup>5</sup>

$$T_C = \frac{1}{2} [(C_a N_{aa} - C_d N_{dd})^2 + 4 C_a C_d N_{ad}^2]^{1/2} - \frac{1}{2} (C_a N_{aa} + C_d N_{dd}) \quad (3)$$

with  $C_j = \frac{n_j(\mu_{eff})^2}{3k_B\mu_0}$ , the effective Curie constant of the  $j$  sublattice, and  $N_{ij} = \frac{2z_{ij}j_{ij}}{n_j g_i g_j \mu_B^2}$  (see Ref. 26). One sees immediately that both the sublattice magnetizations [ $\propto n_j(\mu_{eff})^2$ ] and the exchange integrals ( $J_{ij}$ ) determine the Curie temperatures. According to the theory of superexchange by Anderson<sup>27</sup> with its application to perovskites<sup>28</sup> and taking into account finite one-electron bandwidth,<sup>29</sup> the following functional dependency for the superexchange integral is then determined:

$$j_{ij} = \frac{b^2}{U} \cos^2(\alpha_{ij}/2). \quad (4)$$

Here  $U$  is the Coulomb repulsive energy,  $b$  is the one-electron transfer integral, and  $\alpha$  is the  $\text{Fe}_a\text{-O-Fe}_d$  bond angle. Using the experimentally determined  $\text{Fe}_a\text{-O-Fe}_d$  bond angle (see Fig. 8), it is possible to determine the changes to  $b^2/U$  while changing the stoichiometry. The functional dependence of  $b^2/U$  follows closely the one of  $j_{ad}$  presented in Fig. 10(c). The variation in the bonding angle has only a small influence on the variation in  $j_{ad}$  with the lattice parameter. However, the amplitude of the changes to  $T_C$  is not equivalent for lattice expansion and lattice contraction. Considering Eq. (2), this suggests that also the magnetization changes significantly for reduced lattice parameters, e.g., it needs to be enhanced with respect to the corresponding bulk value. This conclusion is consistent with our previous obser-

vation of a significant magnetization increase for reduced lattice parameters in cation deficient YIG thin films (cf. Ref. 5).

According to theory on superexchange,<sup>27</sup> the exchange integrals  $j_{ij}$  are determined both by the one-electron transfer integral of the  $d$  electrons with the  $p$  electrons of the oxygen anions and the Coulomb repulsion  $U$ . According to Anderson,<sup>27</sup> this parameter  $U$  takes different values corresponding to the valence state of the iron atom, for  $\text{Fe}^{2+}$  and  $\text{Fe}^{3+}$  the Coulomb repulsion  $U$  has been estimated to be equal to 5.8 and  $\sim 10$  eV, respectively.<sup>27</sup> Anderson estimated the one-electron transfer integrals  $b$  to be directly proportional to the crystal electric field splitting characterized by the parameter  $10D_q$ ,<sup>27</sup> with a functional dependence of  $b = A_1 A_2 10D_q = z 10D_q$ , where  $z = A_1 A_2$ . Here  $A_1$  and  $A_2$  represent the normalized relative amplitudes of the orbital in different directions. Anderson has calculated this relation between crystal-field parameter  $D_q$  and  $b$  for  $e_g$  orbitals only (e.g., dominant interaction in perovskites). In order to obtain the exchange integral  $j_{ij}$ , one has to sum the interaction corresponding to all  $d$  electrons ( $=n$ ) of the iron ion. Equation (4) can now be rewritten as follows:

$$j_{ij}^{eff} = \frac{200z^2 \cos^2(\alpha_{ij}/2)}{n^2 U} D_q^2. \quad (5)$$

According to the already presented XANES results, no significant change to the iron valence has been observed within the limits of the experimental accuracy [cf. Fig. 4(b)]. Thus to first order, one can conclude that the Coulomb repulsion  $U$  does not vary significantly with the off stoichiometry for all the studied YIG films. For the following, we shall assume  $U = \text{const}$ . According to Eq. (5), the knowledge of the exchange integral  $j_{ij}$  allows to determine the crystal-field parameter  $D_q$  and notably its variation with off stoichiometry, once the parameter  $U/z^2$  is known. Practically, we shall assume that for a stoichiometric YIG sample, the average parameter  $D_q$  equals  $960 \text{ cm}^{-1}$ .<sup>8</sup> Using this assumption for the stoichiometric YIG film ( $P_{\text{O}_2} = 100 \text{ mTorr}$  and  $a = 12.3746 \text{ \AA}$ ), the parameter  $U/z^2$  equates to a value of  $3.619 \text{ eV}$ . Introducing this parameter  $U/z^2$  into Eq. (5), it is now possible to determine the variation in  $D_q$  with off stoichiometry. Figure 10(c) represents the variation in  $D_q$  with the lattice parameter. For both oxygen deficient and metal-ion deficient YIG films a significant variation in  $D_q$  can be observed. Such a variation in several percents could be confirmed by low-temperature spectroscopic magneto-optics.

## VI. CONCLUSIONS

In this work, we aimed to correlate the change in the intrinsic Curie temperature with the change in the local structure determined by EXAFS and/or the change in iron valence due to oxygen/cation vacancies. On the overall, the relative variations in interatomic distances measured by XAS as a function of stoichiometry are small. However, these measurements are coherent with other results, such as magneto-optical data.  $T_C$  dependence on oxygen and cation stoichiometry is perfectly described using EXAFS measurement results.

The local lattice deformation is found to be different for oxygen and cation nonstoichiometry. The adequacy of the lattice parameter as a measure of oxygen nonstoichiometry has been evidenced. On the contrary, the average lattice parameter seems not to be correlated with the Y/Fe ratio in a bulk sample. The variations in  $a$  and  $T_C$  are relatively small for cation-content variation in the same order of magnitude as oxygen content change.

It can be concluded from XANES and saturation magnetization measurements that  $M_S$  variation is governed by iron site-occupancy change rather than iron-valence variation. Therefore, the large increase in magnetization of thin films with cation vacancies is rather due to specific (octahedral) site iron vacancies, than a change in iron valence. This study explains the large increase in the Curie temperature in cation vacancy thin films in comparison to bulk samples by a  $\text{Fe}_a\text{-O-Fe}_d$  distortion scheme, deduced from EXAFS measurements at the Fe  $K$  edge.

Analysis of the thermal variation in magnetization and magneto-optical Faraday rotation has allowed determining

the microscopic magnetic exchange integrals. Both the magnetization and the exchange integrals are necessary in order to account for the variation in the Curie temperatures with lattice parameters, e.g., with off stoichiometry. Taking into account the absence of a significant variation in the Fe valence with off stoichiometry, it was possible to determine the variation in the crystal-field parameter  $D_q$  with stoichiometry. Magneto-optical spectroscopy would allow to directly determine  $D_q$  and to confirm the invariance of the Coulomb repulsion energy  $U$  with stoichiometry.

## ACKNOWLEDGMENTS

The authors are grateful to V. Cagan (GEMaC) for the precious help with Curie temperature measurements on the bulk samples. We would like to thank F. D'Acapito and Gilda's beamline staff for their help with XAS measurements. W. N. acknowledges a Lebanon CNRS grant.

\*Corresponding author; popova@physique.uvsq.fr

†Present address: NIS, c/o Dipartimento di Chimica IFM, Via P. Giuria 7, 10125 Torino, Italy.

<sup>1</sup>R. Ramesh and D. G. Schlom, *MRS Bull.* **33**, 1006 (2008).

<sup>2</sup>M. A. Gilleo, *Ferromagnetic Materials* (North-Holland, Amsterdam, 1980).

<sup>3</sup>E. Popova, N. Keller, F. Gendron, M. Guyot, M. C. Brianso, Y. Dumont, and M. Tessier, *J. Appl. Phys.* **90**, 1422 (2001).

<sup>4</sup>Y. Dumont, N. Keller, E. Popova, D. S. Schmool, S. Bhattacharya, B. Stahl, M. Tessier, and M. Guyot, *J. Appl. Phys.* **97**, 10G108 (2005).

<sup>5</sup>Y. Dumont, N. Keller, E. Popova, D. S. Schmool, M. Tessier, S. Bhattacharya, B. Stahl, R. M. C. Da Silva, and M. Guyot, *Phys. Rev. B* **76**, 104413 (2007).

<sup>6</sup>Y. Dumont, N. Keller, O. Popova, D. S. Schmool, F. Gendron, M. Tessier, and M. Guyot, *J. Magn. Magn. Mater.* **272-276**, E869 (2004).

<sup>7</sup>B. Vertruyen, R. Cloots, J. S. Abell, T. J. Jackson, R. C. da Silva, E. Popova, and N. Keller, *Phys. Rev. B* **78**, 094429 (2008).

<sup>8</sup>*Magnetic and Other Properties of Oxides and Related Compounds: Garnets and Perovskites*, Landolt-Börnstein, New Series (Springer-Verlag, Berlin, Heidelberg, New York, 1978).

<sup>9</sup>L. G. Van Uitert and F. W. Swanekamp, *J. Appl. Phys.* **28**, 1513 (1957).

<sup>10</sup>D. L. Wood and J. P. Remeika, *J. Appl. Phys.* **37**, 1232 (1966).

<sup>11</sup>D. Elwell and A. Dixon, *Solid State Commun.* **6**, 585 (1968).

<sup>12</sup>E. Popova, N. Keller, F. Gendron, L. Thomas, M. C. Brianso, M. Guyot, M. Tessier, and S. S. P. Parkin, *J. Vac. Sci. Technol. A* **19**, 2567 (2001).

<sup>13</sup>A. Globus, P. Duplex, M. Guyot, and R. Vautier, CNRS Patent No.088 689 (unpublished).

<sup>14</sup>N. Keller, J. Mistrik, S. Visnovsky, D. S. Schmool, Y. Dumont, P. Renaudin, M. Guyot, and R. Krishnan, *Eur. Phys. J. B* **21**, 67 (2001).

<sup>15</sup>J. J. Rehr and R. C. Albers, *Rev. Mod. Phys.* **72**, 621 (2000).

<sup>16</sup>A. Chichagov, D. Varlamov, R. Dilanyan, T. Dokina, N. Drozhzhina, O. Samokhvalova, and T. Ushakovskaya, *Crystallogr. Rep.* **46**, 876 (2001).

<sup>17</sup>F. Hawthorne, *J. Solid State Chem.* **37**, 157 (1981).

<sup>18</sup>G. A. Waychunas, M. J. Apter, and G. E. Brown, Jr., *Phys. Chem. Miner.* **10**, 1 (1983).

<sup>19</sup>L. Galois, G. Calas, and M. A. Arrio, *Chem. Geol.* **174**, 307 (2001).

<sup>20</sup>G. Calas and J. Petiau, *Solid State Commun.* **48**, 625 (1983).

<sup>21</sup>T. E. Westre, P. Kennepohl, J. G. DeWitt, B. Hedman, K. O. Hodgson, and E. I. Solomon, *J. Am. Chem. Soc.* **119**, 6297 (1997).

<sup>22</sup>C. Y. Yang, S. M. Heald, J. M. Tranquada, Y. Xu, Y. L. Wang, A. R. Moodenbaugh, D. O. Welch, and M. Suenaga, *Phys. Rev. B* **39**, 6681 (1989).

<sup>23</sup>R. D. Shannon, *Acta Crystallogr., Sect. A: Cryst. Phys., Diffr., Theor. Gen. Crystallogr.* **32**, 751 (1976).

<sup>24</sup>G. Dionne, *J. Appl. Phys.* **41**, 4874 (1970).

<sup>25</sup>P. Hansen, K. Witter, and W. Tolksdorf, *J. Appl. Phys.* **55**, 1052 (1984).

<sup>26</sup>L. Néel, *Ann. Phys.* **3**, 137 (1948).

<sup>27</sup>P. W. Anderson, *Phys. Rev.* **115**, 2 (1959).

<sup>28</sup>P. G. de Gennes, *Phys. Rev.* **118**, 141 (1960).

<sup>29</sup>J. L. García-Muñoz, J. Fontcuberta, M. Saaaidi, and X. Obradors, *J. Phys.: Condens. Matter* **8**, L787 (1996).